2D Sonar Image Reconstruction via Spiral Source-Based Techniques

Rúben Viegas[1], Friedrich Zabel[2], João Gomes[1], and António Silva[3]

[1] Institute for Systems and Robotics/LARSyS, Instituto Superior Técnico, Universidade de Lisboa, Lisboa, Portugal
[2] Marsensing Lda, Faro, Portugal
[3] CISCA, Universidade do Algarve, Faro, Portugal
ruben.viegas@tecnico.ulisboa.pt

Abstract. Underwater imaging plays an essential role in environmental monitoring and exploration but remains challenging due to the limitations of optical systems in low-light conditions. Imaging sonar provides better performance in such environments and over longer distances; however, state-of-the-art systems often rely on complex hardware configurations, increasing cost and energy consumption. This work investigates a novel sonar imaging approach based on spiral acoustic sources, which allow direction-of-departure estimation using minimal hardware in a monostatic setup. By analyzing the departure azimuth of reflected acoustic paths, it is possible to estimate the locations of reflection points and reconstruct 2D images of the environment. An acoustic propagation model (APM) for 3D environments was developed to validate this concept and was experimentally tested in a controlled pool environment. The proposed system successfully detected sections of the pool walls, validating the spiral field-based imaging system, but with some limitations. These promising results support the potential of spiral acoustic sources for low-cost and sustainable underwater sonar imaging systems.

Keywords: Underwater Sonar Imaging, Spiral Acoustic Fields, Acoustic Propagation Model, Channel Impulse Response Estimate

1 Introduction

Underwater imaging systems play a crucial role not only in exploring underwater environments with autonomous or remotely operated vehicles [1], but also in promoting ocean sustainability by enabling detailed monitoring of marine ecosystems and assessing human impacts [2]. Optical underwater images are often unclear due to low ambient light and turbidity in many environments [3]. In contrast, imaging sonar systems perform better over longer distances and in low-light conditions [4]. State-of-the-art imaging sonar systems typically require at least one of the following: (i) multiple acoustic sources [5], (ii) multiple acoustic receivers [6], or (iii) moving parts [7]. While these features enhance imaging capabilities, they also drive up system costs due to increased equipment, integration complexity, and maintenance demands. Moreover, they can significantly impact sustainability by increasing energy consumption, requiring more raw materials, and generating greater operational and environmental footprints over time.

Spiral acoustic fields allow the direction of sound emission to be determined by analyzing signal phases [8]. This principle has been used in novel underwater localization systems [9, 10]. To generate these fields, a spiral acoustic source is needed – either physically shaped as a spiral [11] or using phased vibrant elements [12–16] – to produce reference/circular and spiral fields. These specialized sources make it possible to compute the direction of departure for different acoustic paths using a single transmitter/receiver pair.

Spiral fields were also used for non-imaging target detection sonar, showing that reflected target paths can still be used to compute directions properly [17]. Since with a spiral source it is possible to obtain the departure azimuth of each acoustic path, theoretically it is possible to locate the reflection points of the environment with a monostatic setup (source and hydrophone collocated). Using all the detected reflection points, it is possible to generate an image of the surrounding environment, enabling the development of novel sonar imaging systems. This could offer a low-cost and more sustainable solution due to its simple hardware requirements and would support, for example, the exploration of confined underwater environments and underwater caves using autonomous or remotely operated vehicles, where signal detection is particularly challenging due to severe multipath effects.

This work presents simulation and experimental results of the concept of using an underwater spiral acoustic source to reconstruct 2D confined environments using imaging techniques. The proposed system is described in Section 2. The developed simulation model is described in Section 3 and the simulation and experimental results are shown in Section 4. Section 5 summarizes the main findings and discusses future work.

2 2D Image Reconstruction using a Spiral Source

This section presents the technical details of the proposed imaging system. Figure 1 shows the flowchart of the data model of the developed system. The input signal, $x(t)$, is transmitted by the spiral source in circular and spiral mode. Since each field has different phase properties, there is a channel impulse response (CIR) for each field, $h_c(\tau)$ and $h_s(\tau)$, which are similar but not exactly the same due to the phase properties of the fields in question. These are not directly available but can be estimated by pulse compression. After the convolution of $x(t)$ with each CIR, the underwater environment also adds noise to the acoustic signal: $w_c(t)$ and $w_s(t)$. The hydrophone receives two signals, $y_c(t)$ and $y_s(t)$, that are used to compute the CIR estimates, $\hat{h}_c(\tau)$ and $\hat{h}_s(\tau)$, by cross correlation with $x(t)$. The fusion CIR, $\hat{h}(\tau)$, is then computed based on the two CIR estimates. The multipath content is extracted from $\hat{h}(\tau)$ to compute the point cloud that represents the 2D surroundings. At this stage, the local reference frame is rotated based on the orientation of the spiral source, ensuring that the estimated positions are properly aligned with the global reference frame. The output image, i.e., the 2D environment estimate, is finally computed based on the previously computed point cloud. The goal of the system is to match the output image with the underwater acoustic channel of the environment.

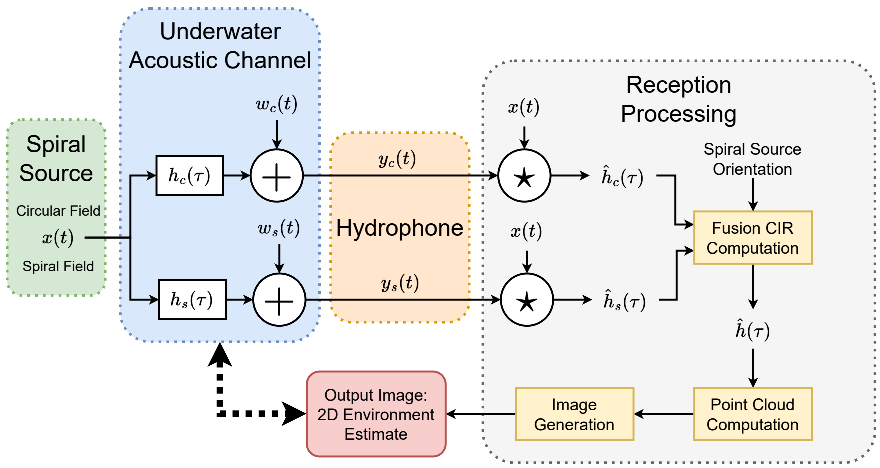

Fig. 1: Flowchart of the data model of the developed system. The input signal, $x(t)$, is transmitted by the spiral source in circular and spiral mode. Since each field has different phase properties, there is a CIR for each field: $h_c(\tau)$ and $h_s(\tau)$. After the convolution of $x(t)$ with each CIR, the underwater environment also adds noise to the acoustic signal: $w_c(t)$ and $w_s(t)$. The hydrophone receives two signals, $y_c(t)$ and $y_s(t)$, that are used to compute the CIR estimates, $\hat{h}_c(\tau)$ and $\hat{h}_s(\tau)$, by cross correlation with $x(t)$. The fusion CIR, $\hat{h}(\tau)$, is then computed based on the two CIR estimates. The multipath content is extracted from $\hat{h}(\tau)$ to compute the point cloud that represents the 2D surroundings. In this step it is necessary to account for the orientation of the spiral source so that the estimated locations are in agreement with the global reference frame. The output image, i.e., the 2D environment estimate, is finally computed based on the previously computed point cloud. The goal of the system is that the output image to match with the underwater acoustic channel of the environment.

For simplicity, in the following, all signals are assumed to be converted to baseband. The received signal $y_c(t)$ is given by

$$y_c(t) = x(t) * h_c(\tau) + w_c(t), \tag{1}$$

where $*$ represents convolution. Similarly, received signal $y_s(t)$ is given by

$$y_s(t) = x(t) * h_s(\tau) + w_s(t). \tag{2}$$

The CIR estimate $\hat{h}_c(\tau)$ is given by

$$\hat{h}_c(\tau) = y_c(t) \star x(t), \tag{3}$$

where $\star$ represents cross-correlation. Likewise,

$$\hat{h}_s(\tau) = y_s(t) \star x(t). \tag{4}$$

The fusion CIR, $\hat{h}(\tau)$, is given by

$$\hat{h}(\tau) = 0.5 \left(\left| \hat{h}_c(\tau) \right| + \left| \hat{h}_s(\tau) \right| \right) e^{j \arg \hat{h}_s(\tau)} e^{-j \arg \hat{h}_c(\tau)} e^{-j\varphi} \tag{5}$$

where arg represents the complex argument of a complex number, and φ represents the orientation of the spiral source, which can be obtained using a compass, for example. The fusion CIR represents a mean absolute value CIR and a phase difference CIR between the two fields. This means that its absolute value can be used to identify acoustic paths and that the complex argument represents the departure azimuth of each acoustic path.

The developed system operates under the assumption that there is no synchronization between the transmitter (TX) and receiver (RX). Consequently, the direct acoustic path – identified as the main propagation path – is used as a timing reference to estimate the exact moment of signal transmission. It is assumed that this direct path corresponds to a known, fixed TX-RX distance, which enables the system to calculate the transmission time based on the known speed of sound in water. This process effectively aligns the estimated impulse response $\hat{h}(\tau)$ in time, enabling accurate determination of the propagation delays for the other signal paths.

The point cloud that represents the 2D surroundings is computed based on the peaks detected in $\hat{h}(\tau)$. Each peak represent a candidate acoustic path and has an amplitude $\hat{a}_i$, a complex argument $\hat{\theta}_i$, that represents the departure azimuth, and a delay $\hat{\tau}_i$. The travel distance of each path is given by $\hat{d}_i = c\hat{\tau}_i$, where c is the sound speed (1500 m/s in this work). Based on the 3D positions of the spiral source and the hydrophone, it is possible to calculate the location of the target that originated a given acoustic path. In monostatic sonar since the spiral source at (x_T, y_T, z_T) is approximately collocated with the hydrophone at (x_R, y_R, z_R), the 2D target position corresponds to a midpoint between the two, and, for the CIR peak i, is given by

$$(x_{M,i}, y_{M,i}) = (x_T, y_T) + 0.5\zeta_i \hat{d}_i \cdot (\cos\hat{\theta}_i, \sin\hat{\theta}_i), \tag{6}$$

where ζ_i is a depth factor given by

$$\zeta_i = \sqrt{\hat{d}_i^2 - |z_T - z_R|^2}. \tag{7}$$

The generation of the output image is done based on the 2D point cloud and the normalized amplitude of each point. In this case, the normalized amplitude is given by

$$\hat{a}'_i = \hat{a}_i \hat{d}_i, \tag{8}$$

in order to compensate for the cylindrical spreading loss. For each point in the 2D point cloud, a circular binary mask with a fixed radius of 0.25 m is created and scaled by the corresponding normalized amplitude $\hat{a}'_i$. These scaled masks are then summed together to form an intermediate image. Finally, a mean filter is applied to the result to generate the output image.

In practice, acoustic paths are often closely spaced or even overlapping in the CIR estimate. To address this issue, it is essential to minimize the peak width in the CIR. Achieving minimal peak width requires maximizing $x(t)$ bandwidth, constrained by the limitations of the spiral source. To facilitate this, time division multiplexing (TDM) is employed to transmit the circular and spiral fields separately. Unlike time-frequency division multiplexing (TFDM), TDM allows full bandwidth allocation to each field by transmitting them at different time instances [18]. In this study, a bandwidth of 23 kHz was selected based on the experimental characterization of the spiral source.

3 Simulation Model Description

The developed simulator computes the arrival features based on the underwater environment and source and hydrophone positions. It is a 3D ray tracing acoustic propagation model (APM) with some simplifying assumptions that are not essential in this work: (i) constant sound speed profile (SSP); (ii) no sound refraction or scattering in the environment; (iii) reflected sound only follows the trajectory of greatest intensity. Figure 2 shows the flowchart of the ray tracing APM, which receives the environment planes, the spiral source and hydrophone positions, and the ray launch directions (directions with equispaced azimuths and elevations). During execution, the model checks if the ray passes in the hydrophone region, and computes the reflection on the intercepted plane. The model outputs the content of the detected arrivals/eigenrays that are used to compute the circular and spiral CIRs, $h_c(\tau)$ and $h_s(\tau)$, respectively.

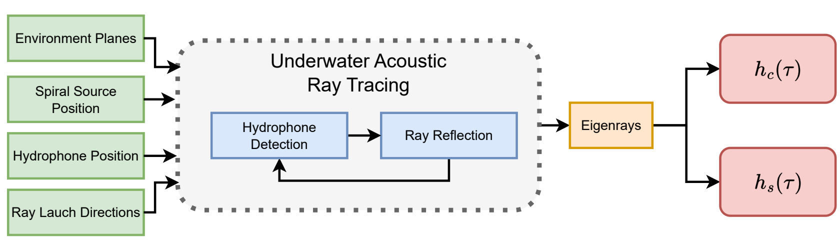

Fig. 2: Flowchart of the developed ray tracing APM, that receives the environment planes, the spiral source and hydrophone positions, and the ray lauch directions. During the execution, the model checks if the ray passes in the hydrophone region, and computes the reflection on the intercepted plane. The model outputs the content of the detected arrivals/eigenrays that are used to compute the circular and spiral CIRs, $h_c(\tau)$ and $h_s(\tau)$, respectively.

Figure 3a shows an example of all detected eigenrays on the pool environment. The model, for each eigenray, outputs the travel time/distance, the azimuth of departure, and amplitude loss due to the plane reflections. The spiral channel frequency response (CFR) is given by [19]

$$H_s(f) = \sum_{i=0}^{N} a_i e^{-2\pi j f \tau_i} e^{-j(\phi_i+\theta_i)} 10^{-L_{\text{thorp}}(f)\tau_i c/20}, \tag{9}$$

where a_i is the amplitude of each ray, τ_i is the delay, ϕ_i is the phase shift, θ_i is the departure azimuth, and $L_{\text{thorp}}(f)$ is the absorption loss using Thorp's empirical formula [20]. The circular CFR is given by (9), with $\theta_i = 0$ due to the constant phase of the circular field along the azimuth. The circular and spiral CIRs, $h_c(\tau)$ and $h_s(\tau)$, respectively, correspond to the inverse Fourier transform of the respective CFR. Figure 3b shows an example of the circular CIR, $h_c(\tau)$ obtained by the eigenrays in red, and its estimate, $\hat{h}_c(\tau)$ obtained by pulse compression in blue, from the developed APM, with SNR of 6 dB.

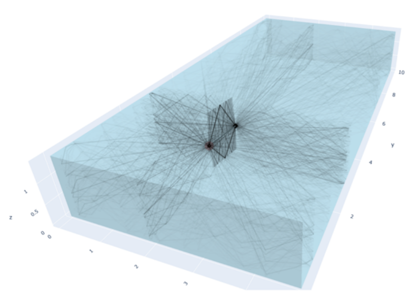

(a)

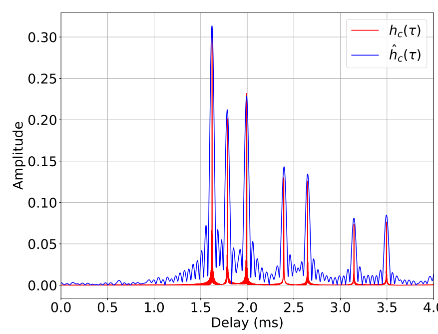

(b)

Fig. 3: Example of a ray tracing simulation. (a) All detected eigenrays on the pool environment. (b) Example of the circular CIR, $h_c(\tau)$ obtained by the eigenrays in red, and its estimate, $\hat{h}_c(\tau)$ obtained by pulse compression in blue, with SNR of 6 dB.

4 Simulation and Experimental Results

This section describes the setup used to carry out simulations with the developed model and to carry out underwater experiments. The simulation and experimental results are presented below.

The underwater experiments to validate the developed system were carried out at University of Algarve, Faro, Portugal, at a scientific outdoor pool with 4.85

by 9.88 by 1.45 meters. Figure 4 shows the developed system with the mentioned pool in the background: spiral source described in [21], a Marsensing digitalHyd TP-1 hydrophone, an underwater container, metal structure, and floats. The structure from the picture, connected to a external supply, was turned upside down and placed on the surface of the pool, allowing easy placement on different positions. A magnetometer was placed above water and attached to the metal structure to determine the orientation of the spiral source, φ.

Fig. 4: Developed system with the experimental pool in the background: spiral source described in [21], a Marsensing digitalHyd TP-1 hydrophone, an underwater container, metal structure, and floats.

Both acoustic equipments were placed at 0.45 m depth and 1.00 m apart, horizontally. The developed system transmitted and received acoustic signals at eight static and known positions. The x-coordinates of these positions were determined based on the measured dimensions of the pool. The TX y-coordinates were calculated using the Time Difference of Arrival (TDoA) between signals received by two static hydrophones placed at the bottom, given the known x-coordinates and hydrophone placements. Since the structure was consistently oriented vertically, the RX y-coordinates were obtained by subtracting the fixed vertical separation of 1.00 m from the corresponding TX y-coordinates.

Linear upward chirps between 17 kHz and 40 kHz of 25 ms duration were transmitted in circular and spiral modes using TDM. Figure 5a shows the output image based on the simulated CIRs for the eight mentioned positions. The simulation results show that the chosen eight positions are not enough to fully reconstruct the pool walls, but they do convey useful information towards that goal.

Figure 5b shows the output image based on the experimental signals. Both figures represent the output image, spiral source, hydrophone, and pool walls positions. The experimental results show that the system was able to roughly detect the left, right and top walls, with similarities to the simulation results.

The bottom wall was not accurately detected, likely due to the lack of positions acquired in its proximity. To improve detection in future experiments, a denser distribution of measurement positions should be adopted.

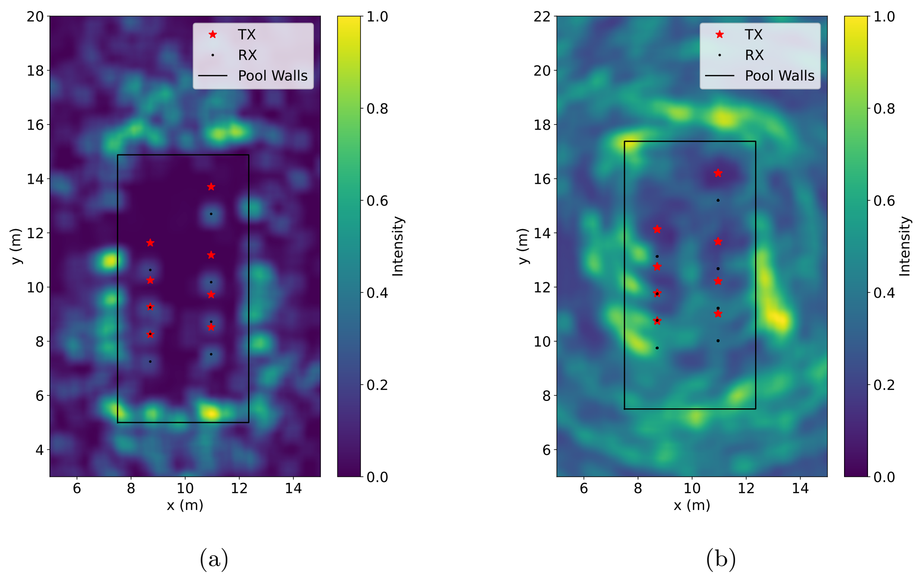

Fig. 5: Imaging sonar comparison between (a) simulation, and (b) experimental results. Both figures represent the output image, spiral source positions (TX), hydrophone positions (RX), and pool walls.

In both images in Figure 5, spurious contamination is visible in the interior region of the pool, possibly due to the approximation required in the computations: considering that the source and the hydrophone are in the same 2D position (monostatic model approximation), when in fact they are 1 meter away. In order to check if this detail is relevant to improve the system, the same simulations as in Figure 5a were performed, but in which the hydrophone was positioned in the same 2D position as the source, at a depth of 0.7 m. Figure 6 shows that the simulation results now have negligible interior contamination. These results confirm that placing the hydrophone as close as possible to the source yields significant improvements under the current monostatic model approximation.

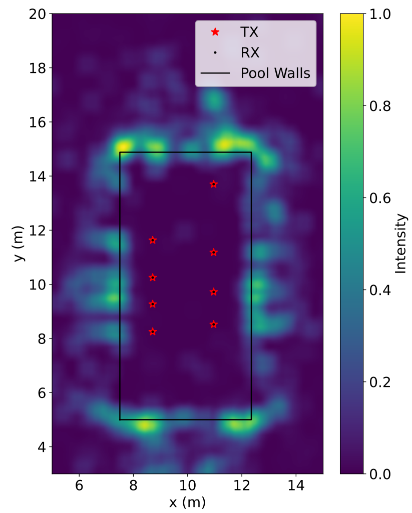

Fig. 6: Imaging sonar simulation results with the hydrophone at the same 2D position as the spiral source. The figure represent the output image, spiral source positions (TX), hydrophone positions (RX), and pool walls.

5 Conclusion

Multiple applications of underwater spiral acoustic fields have been emerging. This work presents the first simulation and experimental results of the concept of using an underwater spiral acoustic source to reconstruct 2D static environments assuming a monostatic setup and using imaging techniques. The system assumes no TX-RX time synchronization, and requires only the TX and RX positions along with the TX orientation. By eliminating the need for multiple time-synchronized sources and/or hydrophones, the system design is significantly simplified. This simplification can lead to a more sustainable solution by reducing both cost and power consumption.

The experimental results where carried out on an outdoor pool with a spiral source and a hydrophone. The reconstructed image shows portions of the pool walls based on the transmission at eight different positions. The developed simulation model was able to predict the portions of the pool walls that were detected experimentally and provide insights on how to improve the image quality in future experiments. Overall, this work presents promising results to develop an effective imaging sonar system using spiral fields.

Future work will explore the effects of assuming a bistatic sonar setup on the computations and, in turn, study the impact of the hydrophone placement relative to the spiral source. Additionally, experiments in static environments with moving transmission and reception systems will be conducted, taking into account the Doppler effect and its influence on spiral wavefronts and image accuracy. To evaluate the performance of the proposed system, comparisons will be made with commercial imaging sonars.

6 Acknowledgement

We would like to thank Instituto Superior de Engenharia (ISE) from Universidade do Algarve (UAlg), namely to Professor Miguel Oliveira for providing the use of the scientific outdoor pool to carry out the acoustic experiments.

This work was supported by LARSyS FCT funding (DOI: 10.54499/LA/P/0083/2020, 10.54499/UIDP/50009/2020, and 10.54499/UIDB/50009/2020).

Rúben S. Viegas is supported by a Portuguese Foundation for Science and Technology grant (DOI: 10.54499/2023.03744.BD).

References

1. Mallios, A., Ridao, P., Ribas, D., Carreras, M., Camilli, R.: Toward autonomous exploration in confined underwater environments: Towards autonomous exploration in confined underwater environments. Journal of Field Robotics 33(7), 994–1012 (Nov 2015)
2. Mariani, P., Quincoces, I., Haugholt, K., Chardard, Y., Visser, A., Yates, C., Piccinno, G., Reali, G., Risholm, P., Thielemann, J.: Range-gated imaging system for underwater monitoring in ocean environment. Sustainability 11(1), 162 (Dec 2018)
3. Hao, Y., Yuan, Y., Zhang, H., Zhang, Z.: Underwater optical imaging: Methods, applications and perspectives. Remote Sensing 16(20), 3773 (Oct 2024)
4. Kim, H.G., Seo, J., Kim, S.M.: Underwater optical-sonar image fusion systems. Sensors 22(21), 8445 (Nov 2022)
5. Smith, M.: Modelling approaches to multibeam echosounders for sound field characterization. The Journal of the Acoustical Society of America 156(3), 1552–1564 (Sep 2024)
6. Hansen, R.E.: Synthetic aperture sonar technology review. Marine Technology Society Journal 47(5), 117–127 (Sep 2013)
7. Ma, B., Du, T., Miyoshi, T.: Environmental mapping of underwater structures based on remotely operated vehicles with sonar system. Journal of Robotics and Mechatronics 35(4), 1092–1100 (Aug 2023)
8. Hefner, B.T., Dzikowicz, B.R.: A spiral wave front beacon for underwater navigation: Basic concept and modeling. The Journal of the Acoustical Society of America 129(6), 3630–3639 (Jun 2011)
9. Dzikowicz, B.R., Hefner, B.T., Leasko, R.A.: Underwater acoustic navigation using a beacon with a spiral wave front. IEEE Journal of Oceanic Engineering 40(1), 177–186 (Jan 2015)
10. Dzikowicz, B.R., Yoritomo, J.Y., Heddings, J.T., Hefner, B.T., Brown, D.A., Bachand, C.L.: Demonstration of spiral wavefront navigation on an unmanned underwater vehicle. IEEE Journal of Oceanic Engineering pp. 1–10 (Jan 2023)
11. Dzikowicz, B.R., Hefner, B.T.: A spiral wave front beacon for underwater navigation: Transducer prototypes and testing. The Journal of the Acoustical Society of America 131(5), 3748–3754 (May 2012)

12. Brown, D.A., Aronov, B., Bachand, C.: Cylindrical transducer for producing an acoustic spiral wave for underwater navigation (l). The Journal of the Acoustical Society of America 132(6), 3611–3613 (Dec 2012)
13. Lu, W., Lan, Y., Guo, R., Zhang, Q., Li, S., Zhou, T.: Spiral sound wave transducer based on the longitudinal vibration. Sensors 18(11), 3674 (Oct 2018)
14. Lu, W., Guo, R., Lan, Y., Sun, H., Li, S., Zhou, T.: Underwater spiral wave sound source based on phased array with three transducers. Sensors 19(14), 3192 (Jul 2019)
15. Viegas, R., Zabel, F., Silva, A.J.: In-lab demonstration of an underwater acoustic spiral source. Sensors 23(10), 4931 (May 2023)
16. Guo, R., Lu, W., Lan, Y.: Underwater acoustic spiral wavefront transducer with low phase directionality error. The Journal of the Acoustical Society of America 156(5), 3459–3467 (Nov 2024)
17. Dzikowicz, B.R., Tressler, J.F., Brown, D.A.: Demonstration of spiral wave front sonar for active localization. The Journal of the Acoustical Society of America 146(6), 4821–4830 (Dec 2019)
18. Viegas, R.S., Zabel, F., Silva, A., Gomes, J.: Underwater localization using time and frequency multiplexing of circular and spiral acoustic fields. In: 2024 Seventh Underwater Communications and Networking Conference (UComms). p. 1–5. IEEE (Sep 2024)
19. Morozs, N., Gorma, W., Henson, B.T., Shen, L., Mitchell, P.D., Zakharov, Y.V.: Channel modeling for underwater acoustic network simulation. IEEE Access 8, 136151–136175 (Jul 2020)
20. Thorp, W.H.: Analytic description of the low-frequency attenuation coefficient. The Journal of the Acoustical Society of America 42(1), 270–270 (Jul 1967)
21. Viegas, R.S., Zabel, F., Gomes, J., Silva, A.: Spiral beacon calibration and experiments for underwater localization. In: OCEANS 2024 - Singapore. p. 1–9. IEEE (Apr 2024)